

Confined Rayleigh-Bénard, Rotating Rayleigh-Bénard, and Double Diffusive Convection: A Unifying View on Turbulent Transport Enhancement through Coherent Structure Manipulation

Kai Leong Chong,¹ Yantao Yang,^{2,3} Shi-Di Huang,¹ Jin-Qiang Zhong,⁴ Richard J. A. M. Stevens,²
Roberto Verzicco,^{2,5} Detlef Lohse,^{2,6} and Ke-Qing Xia^{1,*}

¹*Department of Physics, The Chinese University of Hong Kong, Shatin, Hong Kong, China*

²*Physics of Fluids Group and Max Planck Center Twente, MESA+Institute,*

J. M. Burgers Centre for Fluid Dynamics, University of Twente, 7500 AE Enschede, Netherlands

³*SKLTCs and Department of Mechanics and Engineering Science, College of Engineering, Peking University, Beijing 100871, China*

⁴*Shanghai Key Laboratory of Special Artificial Microstructure Materials and Technology and School of Physics Science and Engineering, Tongji University, Shanghai 200092, China*

⁵*Dipartimento di Ingegneria Industriale, University of Rome Tor Vergata, Rome 00133, Italy*

⁶*Max-Planck Institute for Dynamics and Self-Organization, Am Fassberg 17, 37077 Göttingen, Germany*

(Received 14 February 2017; published 7 August 2017)

Many natural and engineering systems are simultaneously subjected to a driving force and a stabilizing force. The interplay between the two forces, especially for highly nonlinear systems such as fluid flow, often results in surprising features. Here we reveal such features in three different types of Rayleigh-Bénard (RB) convection, i.e., buoyancy-driven flow with the fluid density being affected by a scalar field. In the three cases different stabilizing forces are considered, namely (i) horizontal confinement, (ii) rotation around a vertical axis, and (iii) a second stabilizing scalar field. Despite the very different nature of the stabilizing forces and the corresponding equations of motion, at moderate strength we counterintuitively but consistently observe an enhancement in the flux, even though the flow motion is weaker than the original RB flow. The flux enhancement occurs in an intermediate regime in which the stabilizing force is strong enough to alter the flow structures in the bulk to a more organized morphology, yet not too strong to severely suppress the flow motions. Near the optimal transport enhancements all three systems exhibit a transition from a state in which the thermal boundary layer (BL) is nested inside the momentum BL to the one with the thermal BL being thicker than the momentum BL. The observed optimal transport enhancement is explained through an optimal coupling between the suction of hot or fresh fluid and the corresponding scalar fluctuations.

DOI: 10.1103/PhysRevLett.119.064501

It is very common in nature and engineering settings that, in addition to a driving force, a system is also subjected to a stabilizing force. For a highly nonlinear system, the presence of the stabilizing force may induce surprising phenomena. For instance, Rayleigh-Bénard (RB) convection, which is in nature commonly encountered [1–4] buoyancy driven unstably stratified flow, often experiences a stabilizing mechanism. The first example is RB convection under lateral geometrical confinement (CRB). Here the buoyancy driving interacts with the viscous force from the sidewalls. The second example is RB convection under rotation (RRB) in which the Coriolis force is well known to have a stabilizing effect [5–7]. Our third example is double diffusive convection (DDC) [8], where the fluid density is determined by two scalars with different molecular diffusivities, such as temperature and salinity in the ocean. We consider DDC in the fingering regime, in which the flow is driven by a destabilizing salinity gradient and partly stabilized by the temperature gradient, as in the tropical ocean. All these three systems are of great importance in

astrophysics [9–14], geophysics [15,16], oceanography [17–20], and engineering applications [21].

In these three systems, the stabilizing forces are completely different and correspondingly different physical parameters are required to quantify the degree of stabilization. In CRB, it is the reciprocal of the width-to-height ratio $1/\Gamma$ that characterizes the relative strength of stabilizing [22–24]. In RRB, the stabilization is characterized by the ratio of Coriolis force to buoyancy, which is the reciprocal Rossby number $1/\text{Ro}$ [25–28]. In DDC, it is the ratio of the buoyancy force induced by temperature gradient to that by the salinity gradient, i.e., the density ratio Λ [29,30], that characterizes the relative strength of stabilization. Since the stabilizing mechanisms in the three systems are very different, one would expect that CRB, RRB, and DDC will behave very differently when subjected to the respective stabilizing forces. In this Letter, however, we show that within the parameter range explored the salient features in the three seemingly different systems are universal and can all be explained

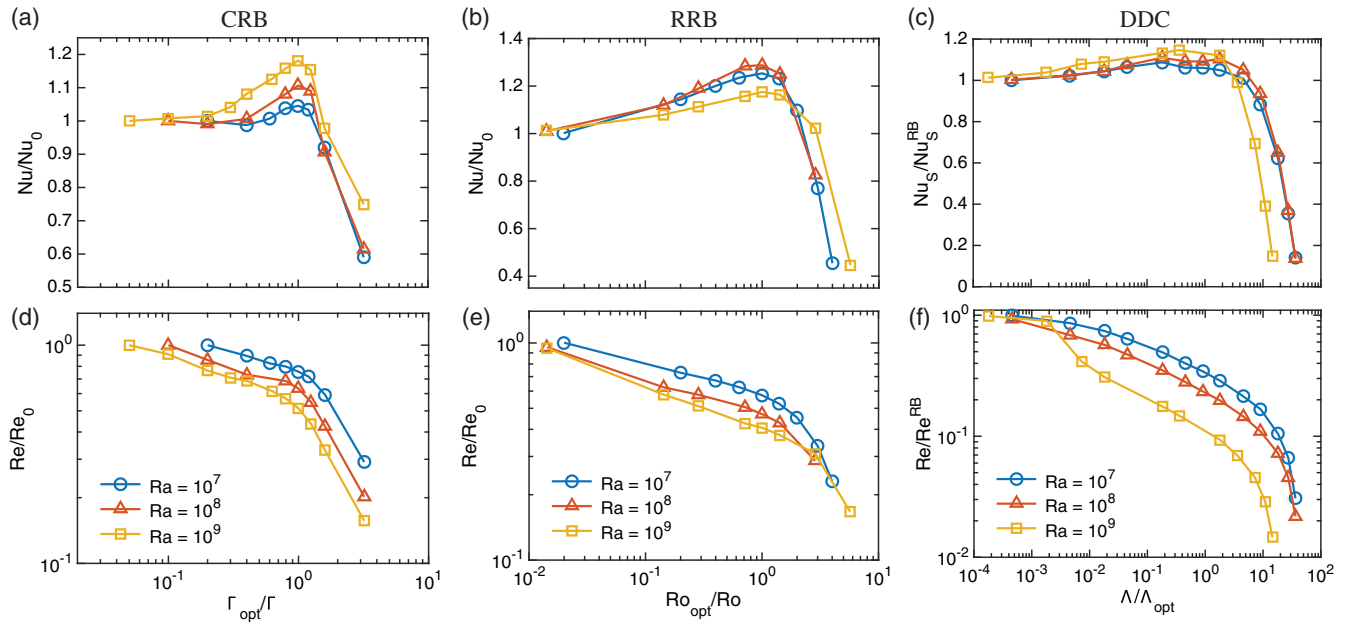


FIG. 1. Nusselt number Nu or Nu_S and Reynolds number Re versus $\Gamma_{\text{opt}}/\Gamma$ for CRB in (a) and (d), Ro_{opt}/Ro for RRB in (b) and (e) and $\Lambda/\Lambda_{\text{opt}}$ for DDC in (c) and (f). Both quantities are normalized by the value obtained from cases $1/\Gamma = 1$, $1/Ro = 0$, or $\Lambda = 0$ (represented by Nu_0 and Re_0 in CRB and RRB and by Nu_S^{RB} and Re^{RB} in DDC).

by coherent structure manipulation and boundary layer crossing and therefore can be understood in terms of a unifying framework.

Our analysis is based on data sets obtained from direct numerical simulations of the three systems. For the simulations, the incompressible Navier-Stokes equation within the Oberbeck-Boussinesq approximations and the convection-diffusion equation(s) are solved for velocities and the scalar field(s), where the Coriolis force and the additional buoyancy gradient generated by a stable temperature gradient are added for RRB and DDC, respectively. The physical quantities are nondimensionalized by the cell height H , the global temperature (or salinity) difference Δ_T (or Δ_S), and the free-fall velocity. The data are taken from our previous simulations reported in Refs. [31–33] for CRB and Refs. [30,34,35] for DDC, respectively. The RRB simulations were conducted by using the numerical solver described in Refs. [36]. The systems are characterized by the Rayleigh number $Ra = \beta_\zeta g \Delta_\zeta H^3 / \nu \kappa_\zeta$ and the Prandtl number $Pr = \nu / \kappa_\zeta$, where g , β , κ , and ν are the gravitational acceleration, expansion coefficient, kinematic viscosity, and molecular diffusivity with the subscript ζ being T (temperature) or S (salinity). Additionally, the Lewis number $Le = \kappa_T / \kappa_S$ is defined for DDC. For each system results for $Ra = 10^7$, 10^8 , and 10^9 are presented. For each Ra , simulations were conducted for a wide range of $1/\Gamma$, $1/Ro$, and Λ . The Prandtl number is $Pr = 4.38$ in CRB, 6.4 in RRB, and 700 (salinity Pr) in DDC. Additionally, in DDC we set the temperature Prandtl number at 7 . In RRB and DDC periodic boundary conditions are applied in the horizontal directions and the box size is set to be much larger than the horizontal width of typical flow structures.

Figure 1 plots the Nusselt number Nu and Reynolds number Re versus the degree of stabilization in the three systems. In CRB and RRB, the heat transport is considered, while in DDC the transport of salinity is considered instead. For the three systems, Nu is evaluated by three different methods introduced in [37,38] while Re is based on the rms of the velocity averaged over the whole domain and time. As the strength of stabilization increases, the global transport behavior undergoes a transition from a typical RB regime to the regime dominated by the stabilizing force. However, earlier studies in CRB [22,24], RRB [26,27,39], and DDC [30,35] separately revealed an intermediate regime with enhanced scalar transport, and in CRB and DDC even the decoupling of scalar and mass transport was observed. Figures 1(a)–1(c) show the normalized Nu against $\Gamma_{\text{opt}}/\Gamma$ for CRB, Ro_{opt}/Ro for RRB, and $\Lambda/\Lambda_{\text{opt}}$ for DDC, respectively. Here $1/\Gamma_{\text{opt}}$, $1/Ro_{\text{opt}}$, and Λ_{opt} are the values of the parameters for which Nu attains its maximum [40]. It is clearly seen that moderate stabilization for all systems can enhance the global heat or salinity transport. Given that the flow weakens monotonically with increasing stabilization [Figs. 1(d)–1(f)], the enhancement is non-trivial and counterintuitive. By comparing the three systems side by side, we can conclude that the leading effect of stabilization is similar: Under moderate strength of stabilization, Nu first increases with increasing degree of stabilization until an optimal state is reached and then excessive stabilization eventually leads to the sharp decline in Nu . From the similarity recognized here we expect that there might be some unifying mechanisms for the systems under distinct forms of stabilizing forces. Indeed a more fundamental understanding on this class of stabilized turbulent flows emerges in this Letter.

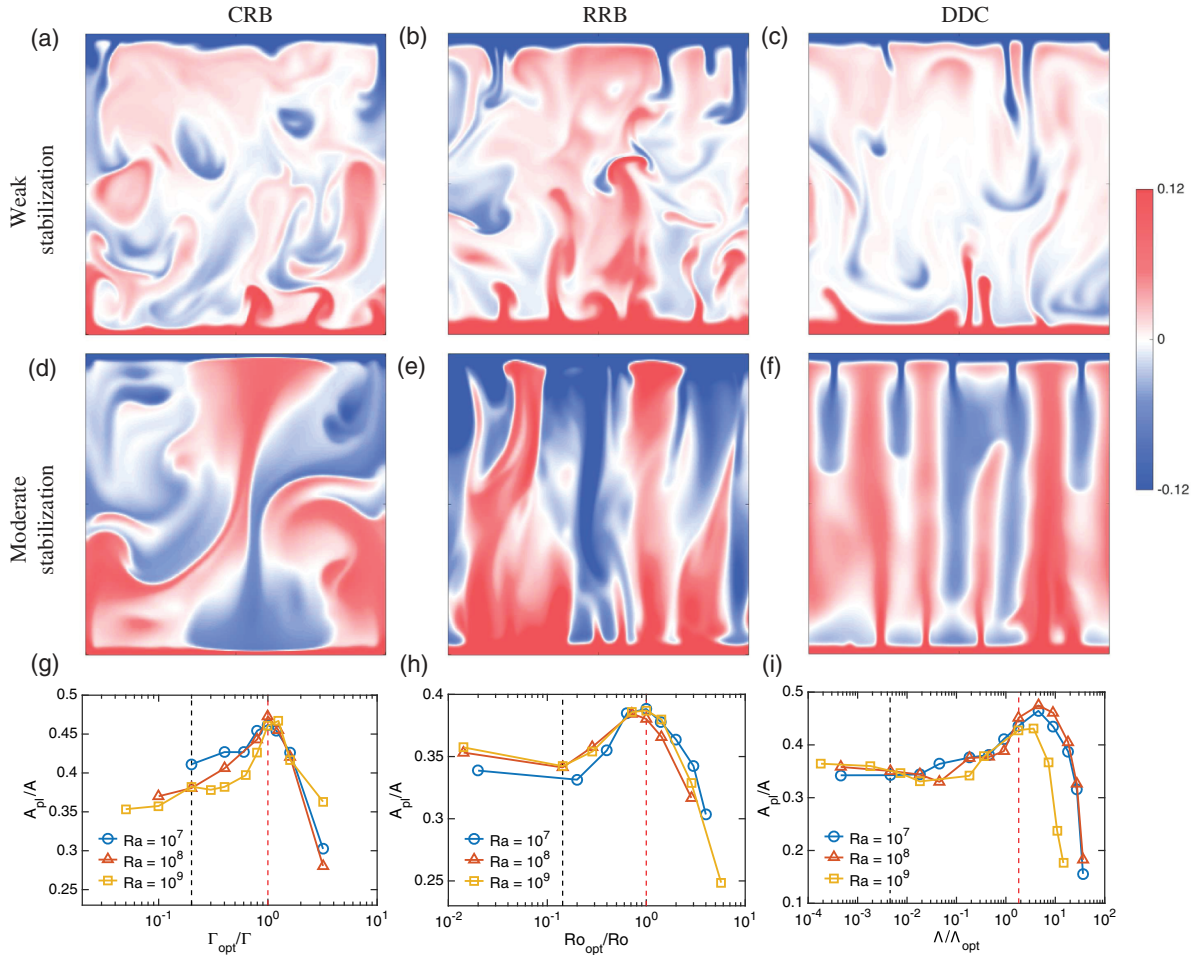


FIG. 2. Instantaneous scalar fields for the three systems (a) $1/\Gamma = 2$, (b) $1/Ro = 1$, (c) $\Lambda = 0.01$, (d) $1/\Gamma = 10$, (e) $1/Ro = 7$, and (f) $\Lambda = 4$ (all at $Ra = 10^8$). The scalar fields are taken at the middle vertical plane and it is midway along the confinement direction in CRB. Here the reddish (bluish) color represents the hot (cold) fluid in CRB and RRB, and the fresher and saltier fluid in DDC. Note that in RRB and DDC, only part of the periodic domain is shown here. Plume coverage A_{pl}/A evaluated at the edge of the thermal or salinity BL versus (g) Γ_{opt}/Γ , (h) Ro_{opt}/Ro , and (i) Λ/Λ_{opt} where A_{pl} is the area covered by cold or saline fluid and A is the total area (see Supplemental Material [41] for the details). Here black (red) dashed lines indicate the cases shown in the top (middle) panel.

We first examine the flow morphologies at the middle vertical plane with weak and moderate stabilization. Figures 2(a)–2(c) show the thermal (or salinity) structures at $1/\Gamma = 2$, $1/Ro = 1$, and $\Lambda = 0.01$ that correspond to the state with moderate scalar transport enhancement and thus the effects of confinement, rotation, and temperature stabilization may be considered to be weak in the respective systems. As seen from Figs. 2(a) and 2(b), for CRB and RRB heat is carried by the mushroomlike plumes that are detaching from the top and bottom boundary layers. When the thermal plumes propagate vertically, their heat content diffuses to the turbulent bulk progressively and their coherence is lost when reaching the opposite boundary layers. In DDC, the salinity structures appear to be more slender than the thermal structures in CRB and RRB because of the large salinity Prandtl number. It is clear from the above observation that under very weak stabilization forces the morphologies of the thermal and salinity structures are similar to that in classical Rayleigh–Bénard flow.

In contrast to the weakly stabilized cases, the flow morphologies can change considerably under stronger stabilization. Figures 2(d)–2(f) show the morphologies at $1/\Gamma = 10$, $1/Ro = 7$, and $\Lambda = 4$, which are cases with maximum Nusselt number in the three systems. As the bulk becomes less turbulent by the respective stabilizing forces, highly coherent structures that extend over the entire height of the cell are formed. We remark that the coherent structures in CRB are still wavy at the optimal state. However, under even stronger confinement the system enters the so-called severely confined regime, with fingerlike, long-lived plume columns [42] similar to those observed in RRB and DDC. The morphological behavior of the plumes may be quantified by the portion of area A_{pl}/A covered by the cold or salty fluid at the edge of the bottom thermal or salinity BL as shown in Figs. 2(g)–2(i). It is seen that moderate strength of stabilization can lead to larger portions of cold or salty plumes covering the bottom plate as compared to the weakly stabilized cases. It also

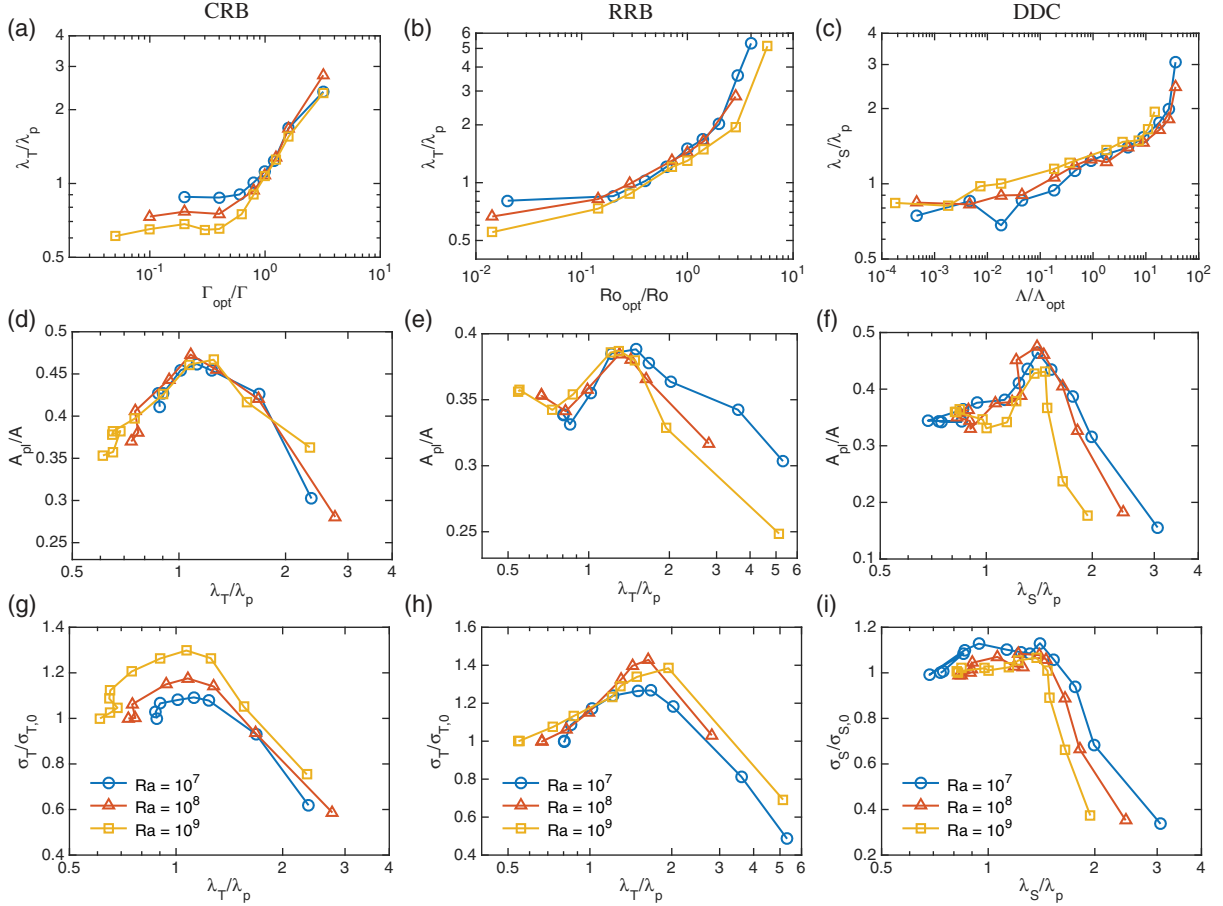


FIG. 3. Ratio of the thermal or salinity boundary layer thickness over momentum one versus (a) $\Gamma_{\text{opt}}/\Gamma$, (b) Ro_{opt}/Ro , and (c) $\Lambda/\Lambda_{\text{opt}}$. Plume coverage A_{pl}/A versus the relative thickness λ_T/λ_p for CRB in (d) and RRB in (e), λ_S/λ_p for DDC in (f). Normalized temperature or salinity standard deviation at the edge of momentum boundary layer versus the relative thickness in (g)–(i).

shows that a too strong stabilization can eventually cause the rapid drop in plume coverage, which coincides with the decline of the global heat or salinity transport. It is therefore clear that highly coherent thermal or salinity plumes are crucial to the enhanced scalar transport, since more coherent structures can better preserve their heat or salt content against thermal or molecular diffusion when traveling to the opposing BL.

We have thus revealed that a hallmark of the stabilizing-destabilizing (*S-D*) turbulent flow is the formation of highly coherent structures. These structures can extend over the height of the cell. In all three systems, the plumes grow from the boundary layer regions that carry the high temperature or salinity anomaly. So we now turn to the effects of the stabilizing mechanism on the boundary layer behaviors. Figures 3(a)–3(c) show the ratio (λ_T/λ_p or λ_S/λ_p) of the thermal or salinity boundary layer thickness over the momentum boundary layer thickness, where the thermal (or salinity) BL thickness λ_T (or λ_S) is defined by the first peak of the temperature (or salinity) standard deviation profile from the bottom and the momentum BL λ_p is defined by the position of the first peak of the $(\partial_x u)^2 + (\partial_y v)^2 + (\partial_z w)^2$ profile, i.e., the location with maximum stress. Note

that the momentum BL is defined through the profile of the stress, which measures fluid suction, and not through the velocity profile (see Supplemental Material [41] for the details). With this definition, which better reflects the physical mechanism at hand here, the edge of momentum BL is the location with the strongest upward suction of hot or fresh fluid near the bottom plate, which is directly related to the heat or salt transfer. The figures show that the BL thickness ratios increase with the increase of stabilization forces and the momentum BL eventually becomes thinner than the thermal or salinity BL. In Figs. 3(d)–3(f) we plot the plume coverage versus the ratio of BL thickness ratio λ_T/λ_p or λ_S/λ_p . It is clear that the plume coverage reaches a maximum (corresponding to the maximum transport enhancement) when the thickness ratio becomes larger than a certain value of order unity and then declines sharply afterwards. To better understand this behavior, we recall that in thermal convection temperature fluctuations reach maximum value at the edge of the thermal BL and then decrease towards the plate [43,44]. From Figs. 3(g)–3(i) one can see that as the momentum BL thickness decreases and becomes close to that of the thermal or salinity one, the temperature or salinity fluctuations reach their maxima. This enables the

coupling of the strongest suction with the maximal scalar fluctuations. It is this coupling that facilitates the emission of coherent structures that is directly responsible for the heat or salt transport enhancement. Once the thickness ratio is much larger than 1, the strongest fluid suction occurs at a layer with largely suppressed scalar fluctuations, i.e., a more stable BL, which explains the subsequent decline in scalar transport. We remark that in some previous studies [25,45–47] BL crossings have been proposed to understand the transition to the rotationally dominated regime in RRB. The present study goes beyond this and enriches the classical picture; it shows that BL crossing leads to an optimal coupling between the suction of hot or fresh fluid and the corresponding scalar fluctuations. Our result also explains why there is no enhancement for those cases in CRB, RRB, or DDC with low Pr or Le numbers [23,30,48], as then the momentum BL is already nested deeply in the thermal or salinity one.

In summary, we have investigated RB flow with a stabilization force using three examples, i.e., the viscous, Coriolis, and negative buoyancy forces. For all three flows we observed significant transport enhancement for moderate values of the stabilizing force. Despite the fact that the nature of the three stabilizing forces is very different, our analysis shows that these forces can similarly influence the coherent structures and the boundary layers. Our study therefore reveals a universal mechanism underpinning scalar transport enhancement in the three types of S - D flows within the parameter range explored. For an appropriate strength of the stabilizing force, the flow structures become more coherent with the vertical motions severely suppressed, resulting in a higher efficiency of scalar transport. It is highly desirable to further investigate this phenomenon for higher values of Ra and Pr. We stress that this class of flow might be generalized to other situations involving different stabilizing forces, such as the Lorentz force in convection with conducting fluid under vertical magnetic field. The ability to understand similar phenomena occurring in different systems under a unified framework has been a hallmark of physics research. The present study of stabilizing-destabilizing flows provides one such example and may therefore inspire work on other systems.

K. L. C., S. D. H., and K. Q. X. acknowledge the Hong Kong Research Grants Council under Grant No. CUHK 404513, a NSFC/RGC Joint Research Grant No. CUHK437/15, and a Hong Kong PhD fellowship. J. Q. Z. was partially supported by a NSFC/RGC Joint Research Grant No. 11561161004. Y. Y., R. J. A. M. S., R. V., and D. L. acknowledge the support from the Dutch Foundation for Fundamental Research on Matter (FOM), and by Netherlands Center for Multiscale Catalytic Energy Conversion (MCEC), a NWO Gravitation program funded by the Ministry of Education, Culture, and Science of the government of Netherlands. The computing resources for CRB were provided by the Leibnitz-Rechenzentrum Munich

under Grant No. pr47vi and the High Performance Cluster Computing Centre, Hong Kong Baptist University, and those for RRB and DDC were provided by the Dutch national e-infrastructure of SURFsara, and the Marconi supercomputer based in CINECA, Italy through the PRACE Grant No. 2016143351.

K. L. C. and Y. Y. contributed equally to this work.

*kxia@cuhk.edu.hk

- [1] G. Ahlers, S. Grossmann, and D. Lohse, Heat transfer and large-scale dynamics in turbulent Rayleigh-Bénard convection, *Rev. Mod. Phys.* **81**, 503 (2009).
- [2] D. Lohse and K.-Q. Xia, Small-scale properties of turbulent Rayleigh-Bénard convection, *Annu. Rev. Fluid Mech.* **42**, 335 (2010).
- [3] F. Chillà and J. Schumacher, New perspectives in turbulent Rayleigh-Bénard convection, *Eur. Phys. J. E* **35**, 58 (2012).
- [4] K.-Q. Xia, Current trends and future directions in turbulent thermal convection, *Theor. Appl. Mech. Lett.* **3**, 052001 (2013).
- [5] J. Proudman, On the motion of solids in a liquid possessing vorticity, *Proc. R. Soc. A* **92**, 408 (1916).
- [6] G. I. Taylor, Motion of solids in fluids when the flow is not irrotational, *Proc. R. Soc. A* **93**, 99 (1917).
- [7] S. Chandrasekhar, *Hydrodynamic and Hydromagnetic Stability* (Clarendon Press, Oxford, 1961).
- [8] T. Radko, *Double-Diffusive Convection* (Cambridge University Press, Cambridge, 2013).
- [9] F. H. Busse, Convection driven zonal flows and vortices in the major planets, *Chaos* **4**, 123 (1994).
- [10] W. J. Merryfield, Hydrodynamics of semiconvection, *Astrophys. J.* **444**, 318 (1995).
- [11] E. Rosenblum, P. Garaud, A. Traxler, and S. Stellmach, Turbulent mixing and layer formation in double-diffusive convection: Three-dimensional numerical simulations and theory, *Astrophys. J.* **731**, 66 (2011).
- [12] J. Leconte and G. Chabrier, A new vision of giant planet interiors: Impact of double diffusive convection, *Astron. Astrophys.* **540**, A20 (2012).
- [13] G. M. Mirouh, P. Garaud, S. Stellmach, A. L. Traxler, and T. S. Wood, A new model for mixing by double-diffusive convection (semi-convection). I. The conditions for layer formation, *Astrophys. J.* **750**, 61 (2012).
- [14] T. S. Wood, P. Garaud, and S. Stellmach, A new model for mixing by double-diffusive convection (semi-convection). II. The transport of heat and composition through layers, *Astrophys. J.* **768**, 157 (2013).
- [15] S. Schoofs, F. J. Spera, and U. Hansen, Chaotic thermohaline convection in low-porosity hydrothermal systems, *Earth Planet. Sci. Lett.* **174**, 213 (1999).
- [16] B. A. Buffett and C. T. Seagle, Stratification of the top of the core due to chemical interactions with the mantle, *J. Geophys. Res. Solid Earth* **115**, B04407 (2010).
- [17] J. Turner, Multicomponent convection, *Annu. Rev. Fluid Mech.* **17**, 11 (1985).
- [18] R. W. Schmitt, Double diffusion in oceanography, *Annu. Rev. Fluid Mech.* **26**, 255 (1994).
- [19] J. Marshall and F. Schott, Open-ocean convection: Observations, theory, and models, *Rev. Geophys.* **37**, 1 (1999).

- [20] R. W. Schmitt, J. R. Ledwell, E. T. Montgomery, K. L. Polzin, and J. M. Toole, Enhanced diapycnal mixing by salt fingers in the thermocline of the tropical Atlantic, *Science* **308**, 685 (2005).
- [21] S. A. Nada, Natural convection heat transfer in horizontal and vertical closed narrow enclosures with heated rectangular finned base plate, *Int. J. Heat Mass Transfer* **50**, 667 (2007).
- [22] S.-D. Huang, M. Kaczorowski, R. Ni, and K.-Q. Xia, Confinement-Induced Heat-Transport Enhancement in Turbulent Thermal Convection, *Phys. Rev. Lett.* **111**, 104501 (2013).
- [23] S. Wagner and O. Shishkina, Aspect-ratio dependency of Rayleigh-Bénard convection in box-shaped containers, *Phys. Fluids* **25**, 085110 (2013).
- [24] K. L. Chong, S. D. Huang, M. Kaczorowski, and K. Q. Xia, Condensation of Coherent Structures in Turbulent Flows, *Phys. Rev. Lett.* **115**, 264503 (2015).
- [25] E. M. King, S. Stellmach, J. Noir, U. Hansen, and J. M. Aurnou, Boundary layer control of rotating convection systems, *Nature (London)* **457**, 301 (2009).
- [26] J. Q. Zhong, R. J. A. M. Stevens, H. J. H. Clercx, R. Verzicco, D. Lohse, and G. Ahlers, Prandtl-, Rayleigh-, and Rossby-Number Dependence of Heat Transport in Turbulent Rotating Rayleigh-Bénard Convection, *Phys. Rev. Lett.* **102**, 044502 (2009).
- [27] R. J. A. M. Stevens, J. Q. Zhong, H. J. H. Clercx, G. Ahlers, and D. Lohse, Transitions between Turbulent States in Rotating Rayleigh-Bénard Convection, *Phys. Rev. Lett.* **103**, 024503 (2009).
- [28] P. Wei, S. Weiss, and G. Ahlers, Multiple Transitions in Rotating Turbulent Rayleigh-Bénard Convection, *Phys. Rev. Lett.* **114**, 114506 (2015).
- [29] M. Kellner and A. Tilgner, Transition to finger convection in double-diffusive convection, *Phys. Fluids* **26**, 094103 (2014).
- [30] Y. Yang, R. Verzicco, and D. Lohse, From convection rolls to finger convection in double-diffusive turbulence, *Proc. Natl. Acad. Sci. U.S.A.* **113**, 69 (2016).
- [31] M. Kaczorowski, A. Shishkin, O. Shishkina, and C. Wagner, Development of a numerical procedure for direct simulations of turbulent convection in a closed rectangular cell, *New Results in Numerical and Experimental Fluid Mech. VI* **96**, 381 (2008).
- [32] M. Kaczorowski and K.-Q. Xia, Turbulent flow in the bulk of Rayleigh-Bénard convection: Small-scale properties in a cubic cell, *J. Fluid Mech.* **722**, 596 (2013).
- [33] M. Kaczorowski, K.-L. Chong, and K.-Q. Xia, Turbulent flow in the bulk of Rayleigh-Bénard convection: Aspect-ratio dependence of the small-scale properties, *J. Fluid Mech.* **747**, 73 (2014).
- [34] Y. Yang, E. P. van der Poel, R. Ostilla-Monico, S. Chao, R. Verzicco, S. Grossmann, and D. Lohse, Salinity transfer in bounded double diffusive convection, *J. Fluid Mech.* **768**, 476 (2015).
- [35] Y. Yang, R. Verzicco, and D. Lohse, Scaling laws and flow structures of double diffusive convection in the finger regime, *J. Fluid Mech.* **802**, 667 (2016).
- [36] R. Ostilla-Monico, Y. Yang, E. P. van der Poel, D. Lohse, and R. Verzicco, A multiple-resolution strategy for Direct Numerical Simulation of scalar turbulence, *J. Comput. Phys.* **301**, 308 (2015).
- [37] E. D. Siggia, High Rayleigh number convection, *Annu. Rev. Fluid Mech.* **26**, 137 (1994).
- [38] R. J. A. M. Stevens, R. Verzicco, and D. Lohse, Radial boundary layer structure and Nusselt number in Rayleigh-Bénard convection, *J. Fluid Mech.* **643**, 495 (2010).
- [39] H. T. Rossby, A study of Bénard convection with and without rotation, *J. Fluid Mech.* **36**, 309 (1969).
- [40] Note that in DDC the optimal state is achieved over a range of density ratios Λ instead of at a single point, and we approximate the optimal value by the midrange.
- [41] See Supplemental Material at <http://link.aps.org/supplemental/10.1103/PhysRevLett.119.064501> for details of plume coverage evaluation, momentum BL extraction and numerical results.
- [42] K. L. Chong and K. Q. Xia, Exploring the severely confined regime in Rayleigh-Bénard convection, *J. Fluid Mech.* **805**, R4 (2016).
- [43] A. Belmonte, A. Tilgner, and A. Libchaber, Temperature and velocity boundary layers in turbulent convection, *Phys. Rev. E* **50**, 269 (1994).
- [44] S.-L. Lui and K.-Q. Xia, Spatial structure of the thermal boundary layer in turbulent convection, *Phys. Rev. E* **57**, 5494 (1998).
- [45] K. Julien, S. Legg, J. McWilliams, and J. Werne, Rapidly rotating turbulent Rayleigh-Bénard convection, *J. Fluid Mech.* **322**, 243 (1996).
- [46] Y. Liu and R. E. Ecke, Heat transport measurements in turbulent rotating Rayleigh-Bénard convection, *Phys. Rev. E* **80**, 036314 (2009).
- [47] E. M. King, S. Stellmach, and J. M. Aurnou, Heat transfer by rapidly rotating Rayleigh-Bénard convection, *J. Fluid Mech.* **691**, 568 (2012).
- [48] R. J. A. M. Stevens, H. J. H. Clercx, and D. Lohse, Optimal Prandtl number for heat transfer in rotating Rayleigh-Bénard convection, *New J. Phys.* **12**, 075005 (2010).